RSC Advances

ROYAL SOCIETY OF CHEMISTRY

www.rsc.org/advances

On the Properties of $Au_2P_3^z$ (z = -1, 0, +1): Analysis on Geometry, Interaction, and Electron Density

Kang-Ming Xu,[1] Shuai Jiang,[1] Yu-Peng Zhu,[1] Teng Huang,[1] Yi-Rong Liu,[1] Yang Zhang,[1]

Yu-Zhou Lv,[1] and Wei Huang[1,2*]

[1]*Laboratory of Atmospheric Physico-Chemistry, Anhui Institute of Optics and Fine Mechanics, Chinese Academy of Sciences, Hefei, Anhui 230031, China*
[2]*School of Environmental Science and Optoelectronic Technology, University of Science and Technology of China, Hefei, Anhui 230026, China*

*E-mail: huangwei6@ustc.edu.cn

Abstract

Au_2P_3, the only metastable binary phase of gold phosphide, has been discovered to exhibit remarkable semiconductor properties among metal phosphides. A systematic study on the geometry, the transformation of Au_2P_3 in different valence states and the different interactions among the atoms of the species is performed by using density functional theory (DFT) method. The global minimum of $Au_2P_3^-$ is a 3D structure with C_s symmetry. This structure could be distorted from a planar configuration of Au_2P_3 with which decreases the steric effect on it and leads to a new stable configuration. An analogous planar configuration, a local minimum rather than a global minimum, is also found in $Au_2P_3^+$, due to the electron effect acting on the structure. Natural bond orbital (NBO) analysis reveals the re-distribution progression of the charge within the species. The central located Au atom and another No. 5 positioned P atoms play significant roles on the structures. P5, as an electron adjuster, balances the electron distribution at different valence states of the structures. Deformation density analysis supplies information about charge transfer and the bonding type between two adjacent atoms as well. Looking deep

insight into the bonding types, as electron localization function (ELF) suggests, the interaction between two adjacent P atoms (P3 and P4) of Au_2P_3 belongs to a strong covalent bond. The Au-P interactions among the configurations could be classified as classical covalent bonds of weak which through the atoms in molecules (AIM) dual parameter analysis. And for the first time, the weak interaction between the two adjacent Au atoms (Au1 and Au2) of the charged states of Au_2P_3 ($Au_2P_3^-$ and $Au_2P_3^+$), are verified and different from the neutral Au_2P_3 through the reduced density gradient (RDG) analysis.

1. INTRODUCTION

Metal phosphides represent a class of promising materials that are widely used with high performance in industrial applications such as phosphide semiconductor materials[1, 2] and processing catalysts.[3-8] Energy harnessing,[9] luminescence,[10] and lithium batteries[11, 12] are among the current innovative applications that have attracted chemists. The bonding scheme of metal phosphides involves metal−metalloid bonds (M−P) involving a strong covalent component. These bonds are usually stronger than those of metal carbides and nitrides.[13] Strong and highly covalent metalloid−metalloid bonds (P−P) are often found in these metal phosphides.

These specific features provide metal phosphides with unique properties, in addition to a wide range of compositions, crystal structures, and accessible electronic states, which allow us to envisage a numerous of novel findings.

Gold is an element that possesses strong relativistic effects.[14-16] Further, its electronegativity is stronger than that of phosphorus, with χ(P) = 2.2 and χ(Au) = 2.5, according to the Pauling scale.[17] Gold phosphides have received significant attention recently, motivated, in part, by the fascinating properties of these materials; indeed, their semi-conductivity and unique optical properties are of particular interest.[18, 19] For the same reasons, a number of experimental[20-26] and theoretical[27-33] investigations have reported on the reactivity of gold phosphides.

The structure of Au_2P_3 has been characterized as a monoclinic phase.[20, 34] Earlier reports indicated that gold phosphides are an air-sensitive metastable binary phase at 1 atm,[35] whereas ternary gold phosphide alloys are stable species.[27, 36, 37] Au_2P_3 belongs to a

class of compounds called "polyphosphides", which process phosphorus-rich phases and P-P bonds.[38] There have been several experimental investigations reported since Au_2P_3 was studied in early work by Haraldsen *et al*.[39] Jeitschko and Möller[20] investigated the Au-Au interaction in the Au_2P_3 crystal structure. Weizer and Fatemi[22] reported the contact resistance of a Au_2P_3 layer, which was found to be very sensitive to the growth rate of the interfacial Au_2P_3 layer. Au_2P_3 was generated in a Au-InP system after sintering at 400 degrees, with a drop of two-to-three orders of magnitude in the contact resistance occurs at the metal-semiconductor interface. Henkes *et al.*[23] reported that Au_2P_3 and other metal phosphides could be synthesized using hot trioctylphosphine (TOP) as the solvent. A study on the generation of $Au_nP_m^{\pm}$ via a Nd:YAG (532 nm) laser was reported by Zheng and co-workers.[24] Recently, Panyala *et al.*[25] also studied $Au_nP_m^{\pm}$ clusters using laser ablation coupled with TOF-MS. Further, Carenco *et al.*[26] recently developed a versatile route for investigating the formation of Au_2P_3 nanostructures using white phosphorus (P_4) as the phosphorus source instead of TOP.

However, to the best of our knowledge, there have been no systematic theoretical studies of Au_2P_3 reported in the literature. A theoretical study focusing on the type of electron and interatomic interactions of Au_2P_3 are likely to be of benefit to the chemical community in realizing the unique properties associated with this species.

Herein, we systematically report a density functional study on the different valence states of Au_2P_3. We give an overall analysis of the electron interaction on the transformation of the different valence state of $Au_2P_3^z$ (z = -1, 0, +1). Additionally, we also describe the different interaction types of these species using different methods of analysis.

2. THEORETICAL METHODS

The basin-hopping (BH) global search method[40-44] coupled with density functional theory (DFT) was employed to search for low-lying isomers of phosphorus-doped clusters of the type $Au_2P_3^z$ (z = -1, 0, +1). The generalized gradient approximation (GGA) in the Perdew-Burke-Ernzerhof (PBE)[45] functional form coupled with double-numerical polarized (DNP) basis set was chosen to carry out the electronic structures calculations in the DMol3 software package.[46] Randomly produced structures of each species were used as the initial inputs for the BH search algorithm, and 200 initial low-lying isomers were generated after 200-300 BH moves. As our early work[32, 33, 47-53] shown the selection and verification on the functional and basis set for Au/P systems, PBE[45] functional coupled with CRENBL basis set used for Au and P was selected for the optimization calculations of the top 10 lowest-lying isomers of each species. Additionally, relative energies of the top 5 isomers were selected for single-point energy calculations at the PBE0[54]/CRENBL level of theory. All approaches were implemented using the NWCHEM 5.1.1 software package.[55, 56]

To explore the transformation between similar structures and the corresponding effects of the electrons, three similar configurations in different value states (i.e. the global minimum of the anionic, the neutral and the second-low-lying isomer of cationic Au_2P_3) were specially selected for further investigation. Natural bond orbital (NBO)[57] analysis of the three isomers was performed with the PBE0/6-311+G*(P)|CRENBL(Au)level of theory as an all electron triple-zeta 6-311+G* basis set substitutes the pseudopotential CRENBL basis set for phosphorus for considering inner electrons effects as implemented in Gaussian 09W software package.[58] Subsequently,

deformation density and electron localization function (ELF),[59, 60] topology analysis of the electron density at the bond critical points (BCPs), and reduced density gradient (RDG)[61] of the Au1-Au2 bond were successively investigated at the more high accuracy of the second-order Møller-Plesset perturbation (MP2)[62] with 6-31+G* basis set for P atom and CRENBL pseudo-potential basis set for Au atom [MP2/6-31+G*(P)|CRENBL (Au)] level of theory. All these calculations were performed using the Multiwfn 3.3.6 program package.[63]

3. RESULTS AND DISCUSSION

This section consists of two parts: The first part includes subsections 3.1 and 3.2, which discuss the transformation of structures at different valence states, and the second part includes subsections 3.3-3.6, which discuss the atomic interactions within $Au_2P_3^z$ (z = -1, 0, 1).

3.1 Equilibrium Structures

To simplify the description of the isomers, the states of the anion, neutral and cation are labelled as 'A', 'N', and 'C', respectively. The different isomers are also labelled with 'I', 'II', 'III', *et al.* according to their relative energy. Arabic numbers indicate the atoms and angles of the clusters, as shown in Figs. 1 and 2. The notation of combination Element and Number, e.g., Au1, represents the element in the number labelled position (see Fig. 2).

The first five low-lying isomers of $Au_2P_3^z$ (z = -1, 0, +1) are listed in Fig. 1. A(I) possesses C_s symmetry with two perpendicular planes that are connected by Au1. In contrast, N(I) possesses a plane configuration with C_s symmetry. The energy difference

between N(I) and N(II) is approximately 0.591 eV and is far beyond the isomer-coexistence interval of 0.1 eV, which coincides with an estimate of the accuracy of the DFT method for gold clusters (deduced from a comparison between the recent mobility measurements and theoretical calculations[64]), indicating that N(I) is the most stable isomer among neutral species. The global minimum of $Au_2P_3^+$ (C_I) is a 3D configuration where one gold atom dangles on the Au-P-P-P moiety constructed within a pseudo-plane connecting a phosphorus atom. C(II) possesses a C_s symmetrical structure that is similar to N(I). Notably, C(II) is 0.299 eV higher in energy than C_I. We note that the two most stable isomers of Au_2P_3 are similar to $Au_2P_3^+$ with the energy ordering reversed. Moreover, N(II) is structurally similar to C(I) and, as noted previously, is 0.591 eV higher in energy than N(I). Further, C(II) is structurally similar to N(I) and is 0.299 eV higher in energy than C_I. A possible conjectured pathway for the inter-conversion of N(I) and C(I) is presented in Fig. S1 (ESI†). It is well known that the rearrangement of electrons can significantly change the structure of a molecule in some situations. In this regard, A(I) is a configuration with a 90° distortion compared with N(I), which is a consequence of the interaction of the additional electron. The loss of one electron from N(I) forms a relatively higher energy configuration. A low energy configuration (i.e. C_I) can be formed through structural rearrangement via the possible transformation path shown in Fig. S1 (ESI†).

A(I), N(I) and C(II) (i. e. the global minimum of $Au_2P_3^-$, the global minimum of Au_2P_3 and the 2nd low-lying isomer of $Au_2P_3^+$) presented in Fig. 2 are chosen for further investigation to examine the transformation between similar structures and the effects made by electrons. It is clear that the three isomers are somewhat different from each

other due to the different valence states. Table 1 shows the atomic distances and angles of these three structures. Compared with the angles within C(II) and N_1, ∠ of N(I) decreases from 54.6° to 51.8° (i.e., approximately 3°) and ∠ increases from 71° to 76.2° (i.e., 5.2°). These changes result in the atomic distance to become elongated by approximately 0.12 Å for the $d_{1\text{-}2}$ bond of C(II) (from 2.742 to 2.860), whereas the value of A(I) is 2.922 Å.

3.2 Natural Bond Orbital (NBO)

The gain or loss of an electron is equal to the increase or decrease of a valence electron, respectively; thus, the atomic charge can reflect the total change of the valence electrons. NBO analysis[57] enables a simple depiction of the chemical bond based on the interaction of orbitals. Table 2 shows the natural electron configuration (NEC) of each Au and P atoms and the atomic charge distribution of $Au_2P_3^z$ (z = -1, 0, +1).

A(I): The extra charge is mostly attributed to P5 and Au1 at -0.553 and -0.221 units of charge, respectively (Table 2). The 6p orbital of Au1 possesses 0.67 unit of charge which is mainly contributed from three parts. The first part is from the 6s and 5p orbitals through *spd* hybrids. Considering the strong relativistic effect of Au, the energy gap between the valence 6s and 5d orbitals diminishes significantly. At the same time, 5p and 5s orbitals are relativistically stabilized and 5d orbitals destabilized. As a result, the 6s-5d energy gap was reduced and s-p-d hybridization was enhanced. The second part is from the negative charge obtained from outside, this part could contribute 6d orbital at most 0.221 unit of charge as no more than the total charge on Au1. The third part is that some charge could be transferred from other atoms like the connected gold or phosphorus atoms due to the interactions of atoms. But there is a little hard to distinguish the

contribution of each part. The 3s orbital of each P atom may also transfers charge to 3p orbitals with s-p hybridization occurring. A point that should be mentioned is that the 3p orbital of P5 receives -0.553 unit of charge, and the NEC of this atom is $3s^{1.81}3p^{3.71}3d^{0.01}4p^{0.01}$. There are twice as many electrons in the 3p orbital than in the 3s orbital, which is consistent with the sp^2 hybrid feature.

N(I): In this electrically neutral structure, the negative charge is distributed on Au1 and P5, with -0.182 and -0.183 units of charge, respectively. The Au2 atom could transfer electrons to Au1 and P5, and the inner 6s and 5d orbitals of Au1 co-transfer charge to the 6p orbital. Additionally, Au1 accepts 0.182 unit charge from other neighboring atoms.

C(II): Though this species is deficient by one electron relative to A(I) and N(I), the Au1 still acts as an electron acceptor. This may be due to the strong electron affinity (EA) of Au, is 2.309 eV, which is not qualitatively different from that of iodine, 3.059037 eV.[65] Thus, even in ionic compounds, in which Au acts as an electron acceptor. The Au1 shows a strong tendency to attract electrons, but Au2 is still a qualified electron donor. Compared with N(I), the P5 donates 0.296 units of charge to become an electron donor instead of an acceptor, as it was in N(I).

Overall, moving from C(II) to N(I) to A(I), P5 transitions from being an electron donor to an acceptor. The P5 acts as an electron adjuster with excess electron to store and less electron to release (Table 2). The electrons of P5 mainly occupy the 3p orbital when the charge transfer occurs. The two gold atoms of the isomers are quite different with the centered Au1 always acting as an electron acceptor and Au2 acting as an electron donor.

We can interpret the structural transformation from N(I) to A(I) in terms of the location of the electron in P5. Plane 1-2-5 rotates 90° to decrease its electron repulsive interaction, resulting in a 3D configuration of C_s symmetry in A(I). For a more direct view of the orbital interactions, four high occupied molecular orbitals are presented in Fig. 3. A(I) is a closed-shell structure, whereas N(I) is an open-shell structure processing a single occupied molecular orbital (SOMO). The HOMO and LUMO of N(I) are similar to those of A(I)，but the HOMO-1 shows a large difference between these structures. The HOMO-1 of N(I) shows that Au1-P3-P4 form a three-atom π orbital. C(II), which possesses one less electron than N(I), is a closed-shell structure. The MOs of C(II) possesses one less shell orbital compared with that of A(I). The electrons of the inner orbitals in HOMO-3 of A(I)/HOMO-2 of C(II) are donated to the Au2 *d* orbitals (Fig. S2, ESI†). This demonstrates that the interaction of an electron could significantly change the scheme of the atomic orbitals that form molecular orbitals.

3.3 Deformation Density Analysis

The electron density deformation function is defined as the difference between the total electron density of the molecule and electron densities of each separated atom. To qualitatively understand the nature of the Au-P interaction, a graphical representation of the electron density deformation upon the formation of the interactions between the Au and P atoms is shown in Fig. 4. The positive and negative density differences are represented by cyan solid and purple dashed lines, respectively, which represent the accumulation and depletion of electron density from the separated atoms to the atoms in the molecule. The density difference map provides direct insight into the effect of electron transfer and the change in bonding.

For simplicity, we first describe N(I) in Fig.4b, for which several points can be concluded. There is a large loss of electron density in the nucleus region of the gold atoms, and the remaining charge attracted by the nucleus collapses inward and splits into two parts. The electron density accumulates between the gold atom and the phosphorus atom (i.e., Au1-P3, Au1-P4, Au1-P5 and Au2-P5), which indicates the existence of an interaction between the gold and phosphorus atoms. No electron density accumulates between Au1 and Au2, indicating that the interaction between these two atoms is rather weak and no covalent bond character is present. However, in contrast to Au1-Au2, there is a large accumulation of electron density between P3-P4, which indicates that a strong bond is formed between these two P atoms. Next, we compare the electron density deformation of N(I) with that of A(I) and C(II).

N(I) vs C(II) (Fig. 4b vs Fig. 4c): C(II) may be regarding as N(I) but with the removal of one electron. As seen in C(II), P5 possesses positive electron density deformation around the negative nucleus region. The Au2 possesses large negative electron density in the region of the nucleus. The charge between Au2 and P5 is low. This may cause the electron attractive force from P nucleus to become stronger following the loss of one electron. Subsequently, the original electron localized in interatomic of Au2-P5 is now distributed to the P5 atom. This means that the interatomic interaction is weak and does not possess the covalent bond character.

N(I) vs A(I) (Fig. 4b vs Fig. 4a'/4a): As mentioned above, N(I) is a stable structure, and its SOMO can accept an additional electron to form a closed-shell structure. A structure with an open-shell electron configuration will rearrange to more stable structure with a closed-shell electron configuration when it receives an additional

electron. In this case, the addition of an electron to N(I) causes electron density to be transferred from P5 to Au2.

Because A(I) possesses a 3D configuration of C_s symmetry, we have selected two perpendicular planes to describe it. Plane 1-3-4 and plane 1-2-5 are presented in Figs. 4a and 4a', respectively. If we compare N(I) with A(I), we find that the P atoms have obtained charges to a different extent. There is a trend of electron density transferred from phosphorus to gold. For A(I), the density of Au1 relative to the other four atoms becomes larger following the addition of the electron.

3.4 Electron Localization Function (ELF)

ELF[59, 60] has been used to investigate the pair electron distributions and bonding properties of $Au_2P_3^z$ (z = -1, 0, +1) as it may provide an absolute characterization of covalency versus ionicity.

Core basins are located around the nuclei and valence basins are characterized by their synaptic parts. Monosynaptic basins represent lonely electron pairs (LPs), whereas di-synaptic basins represent covalent bonds.[67] Fig. 5 clearly characterizes the core and valence basins around the Au and P atoms. A di-synaptic basin between P3 and P4 shows a strong covalent interaction in inter-phosphorus atoms (Fig. 5a', 5b, and 5c). We note that this strong covalent interaction is also consistent with the definition of a "polyphosphide". No di-synaptic basin is found between Au and P, suggesting the presence of non-covalent bonds. Each P atom possesses a monosynaptic basin, which indicates the presence of their lonely electron pairs. The crescent shaped basin is removed from the interaction regions among the atoms because of the electron repulsive

interaction. According to the calculated ELFs, essentially no electron pairing density exists between the Au1 and Au2 atoms and other Au-P interactions. The interaction of these will be discussed below.

3.5 Topology analysis

Bader's atoms in molecules (AIM) theory,[67] which is based on a topology analysis of the electron density ($\rho(r)$) and its Laplacian ($\nabla^2\rho(r)$), has been widely applied in the study of intermolecular interactions. The topology analysis of the electron density has shown that the critical point of (3, -1) appears to be, in general, located between attractive atom pairs; hence, it is commonly referred to as the bond critical point (BCP). The chemical bonding can be characterized by the existence of a (3,-1) type of BCP and its corresponding bond path. In Table 3, the electron density $\rho(r)$ of each pair of atoms is above zero and in the proposed range 0.053–0.144. The Laplacian of the electron density ($\nabla^2\rho(r)$) ranging from -0.208 to 0.117, is simply the sum of the three curvatures of the density at the critical point (i.e., λ_1, λ_2, and λ_3). Generally, a negative Laplacian indicates that the electronic charge is concentrated in the inter-nuclear region and, therefore, shared by two nuclei. This type of situation occurs in all shared electron interactions (i.e., covalent or polar). A positive value reveals a local excess in kinetic energy and indicates depletion of electronic charge in the region. This type of situation occurs in all closed shell interactions (i.e., ionic bonds, hydrogen bonds, or van der Waals interactions).[67] As seen in Table 3, the Au2-P5 interaction of N(I) and P3-P4 interaction in all three configurations have negative Laplacian. We note that more negative values are indicative of a stronger covalent bond. Relative to A(I) and C(II), the P-P covalent bond of N(I) is

the strongest. In contrast to N(I), positive Laplacian for the Au2-P5 interaction are obtained for A(I) and C(II). As defined, the interaction between these moieties should not be regarded as a covalent bond. Indeed, the Laplacians between the Au and P atoms are all small and positive. One must then ask: To what type of bond do these interactions belong? To address this question, energy based considerations are warranted. In particular, the relationship between the total electronic energy densities at the BCPs (E(r)), the kinetic energy densities (G(r)), and the potential energy densities ($\mathcal{V}$(r)) must be considered, as indicated by equation (1). Here, E(r) is negative for covalent bonds (i.e., $\nabla^2\rho(r) < 0$), whereas it is positive for ionic bonds (i.e., $\nabla^2\rho(r) > 0$).

$$E(r) = G(r) + \mathcal{V}(r) \qquad (1)$$

$$2G(r) + \mathcal{V}(r) = \left(\frac{\hbar^2}{4m}\right)\nabla^2\rho(r) \qquad (2)$$

$$E(r) = \left(\frac{\hbar^2}{4m}\right)\nabla^2\rho(r) - G(r) \qquad (3)$$

Given equation (2), which describes the relationship between G(r) and $\mathcal{V}$(r), E(r) may still be negative in equation (3) if the Laplacian $\nabla^2\rho(r)$ is positive. This situation may occur if the kinetic energy density G(r) is consistently positive. At the BCP, some region should exist where $E(r) < 0$ but $\nabla^2\rho(r) > 0$. Nakanishi[68] proposed an AIM dual parameter analysis to better understand weak to strong interactions involving total electron energy densities E(r) and the Laplacian of the electron densities $\nabla^2\rho(r)$. Negative E(r) and positive $\nabla^2\rho(r)$ characterize an intermediate interaction between shared-shell (i.e., $E(r) < 0$, $\nabla^2\rho(r) < 0$) and purely closed-shell (i.e., $E(r) > 0$, $\nabla^2\rho(r) > 0$) interactions. Typical ranges of the electron density and electron energy density at BCPs were also examined

for the classical covalent bond of weak interactions: $0.05 < \rho < 0.17$ and $-0.13 < E(r) < -0.03$. In Table 3, the Laplacians of Au-P at the BCP are all positive, and their corresponding energy densities E(r) are all negative and are ranged from approximately -0.13 to -0.03. Therefore, the present Au-P interaction could be referred as covalent bonds of weak (Cov-w).[68]

The ellipticity of the electron density at the BCP is based on AIM analysis.[66, 67] It is a useful chemical index in the description of unusual bonds in charge transfer interactions, steric contacts, etc. The parameter provides a quantitative measure of the anisotropy of the electron density at the BCP.

Ellipticity, ε, is described as:

$$\varepsilon = \lambda_1 / \lambda_2 - 1 \qquad (4)$$

in which $\lambda_2 < \lambda_1 < 0$, λ_i (i = 1, 2) are the eigenvalues of the corresponding eigenvectors $\mathbf{v}_1$ and $\mathbf{v}_2$ of the Hessian matrix of ρ(r) (Fig. 6). The values of λ_1 and λ_2 on Au1-Au2 of N(I) are -0.036 and -0.017, respectively. The ε value is 1.132 which is obviously abnormal compared with the other values shown in Table 3. Fig.6 shows a direct view of the ellipticity at the BCP of Au1-Au2. The abnormal ε value indicates a strong polarization of the BCP, and the interaction is very complex.

3.6 Reduced Density Gradient (RDG)

RDG analysis[61] method is very important and also an excellent method to examine weak interactions. It can be viewed as an extension of AIM theory, and it is used in many fields where the AIM theory is not suitable, such as π-π accumulation, the

absence of BCPs, etc. In our species, a BCP was not found on Au1-Au2 in either A(I) or C(II). Weak interactions can be isolated as regions with low electron density and a low RDG value. The electron density values of the low-gradient spikes [plot of RDG vs sign(λ_2)ρ] indicate the interaction strength. The plot of the RDG versus the electron density ρ multiplied by the sign of λ_2 can be used to analyzed and visualize a wide range of interactions types. A plot of the RDG versus sign(λ_2)ρ for Au1-Au2 of A(I), N(I) and C(II) are presented in Fig. 6. As shown, the Au1-Au2 interaction in N(I) has a BCP, whereas BCPs for A(I) and C(II) are not present because the RDG values are greater than zero. The characteristic peaks directed toward the sign(λ_2)ρ values are 0.041 (A(I)), 0.052 (N(I)), and 0.044 a.u (C(II)). These low values indicate that there are very weak interactions between Au1 and Au2. The low RDG values (see in Fig. 7) coupled with the low positive density differences between Au1 and Au2 (see in Fig. 3a', 3b and 3c) denote covalent bond character and indicate that the interaction type belongs to one that is very weak. The strength of the interaction is a function of bond distances, as the typical understanding of the interaction is inversely proportional to the corresponding distance of Au1-Au2. Compared the bond distance between Au1 and Au2 of Au_2P_3 species with pure Au_2 cluster at different value states (Table S1), the distance of Au_2P_3 is longer than that of Au_2, and the weak interaction of Au1-Au2 in Au_2P_3 species could be also proved.

4. CONCLUSION

We report a systematic theoretical study on the transformation of Au_2P_3 at three different valence states as well as the different interactions among the atoms of these species. A(I) is shown to be a 3D structure that may distored from a planar structure like N(I). C(II) releases to a lower energy configuration C(I) through the structural

rearrangement and the transfer former is possibly N(I). NBO analysis reveals the re-distribution of natural charge following inter-conversion between these species. The Au1 and P5 atoms play vital roles in the transformation of the structure following the gain and loss of an electron. P5 adjusts the angles and distances to generate new configurations with higher stability. ELF shows a visualized description of the bonding type in Au_2P_3, in which the interaction between P3 and P4 can be considered to be a strong covalent bond. Topology analysis indicates that the interaction type between the Au and P atom is testified as Cov-w. A RDG analysis indicates that no BCPs between Au1 and Au2 in A(I) or C(I) are present. Further, weak covalent interactions between Au1 and Au2 among the three different isomers have been identified. The present investigation on the electron interaction of the different valence states of $Au_2P_3^z$ (z = -1, 0, +1) and the different interaction types within these species may help guide future theoretical and experimental investigations of these structures and provide new insights for the synthesis of new materials.

ACKNOWLEDGEMENTS

The study was supported by grants from the National Natural Science Foundation of China (Grant No. 21403244 and 21133008), the National High Technology Research and Development Program of China (863 Program) (Grant No. 2014AA06A501). "Interdisciplinary and Cooperative Team" of CAS. Acknowledgement is also made to the "Thousand Youth Talents Plan". The computation was performed in EMSL, a national scientific user facility sponsored by the department of Energy's Office of Biological and Environmental Research and located at Pacific Northwest National Laboratory (PNNL). PNNL is a multiprogram national laboratory operated for the DOE by Battelle. Part of the

computation was performed at the Supercomputing Center of the Chinese Academy of Sciences and Supercomputing Center of USTC.

Table 1. **The bond lengths and angles of A(I), N(I) and C(II). All bond lengths are given in angstroms and angles are given in degrees.**[a]

Isomer	∠1	∠1′	∠2	∠3	∠4	∠5	∠1″	d_{1-2}	d_{1-3}	d_{1-4}	d_{1-5}	d_{2-5}	d_{3-4}
A(I)	52.1	51.4	50.4	64.3	64.3	77.5	127.1	2.922	2.503	2.503	2.308	2.362	2.166
N(I)	54.6	48.9	54.4	66.3	64.8	71.0	112.2	2.742	2.443	2.474	2.359	2.362	2.036
C(II)	51.8	50.8	52.0	64.1	65.1	76.2	109.9	2.860	2.526	2.506	2.320	2.315	2.158

[a] The atomic distance and angle notations correspond to those labelled in Fig. 1(i.e., A(I)).

Table 2. **Natural electron configuration and charge distributions of each atom for the three valence states of Au_2P_3 at the PBE0/6-311+G* level of theory.**

Species	Atom	No.	Charge	Natural Electron Configuration
A(I)	Au	1	-0.221	$6s^{0.88}5d^{9.65}6p^{0.67}7s^{0.01}6d^{0.01}$
	Au	2	0.014	$6s^{1.07}5d^{9.84}6p^{0.07}$
	P	3	-0.120	$3s^{1.80}3p^{3.29}3d^{0.02}4p^{0.01}$
	P	4	-0.120	$3s^{1.80}3p^{3.29}3d^{0.02}4p^{0.01}$
	P	5	-0.553	$3s^{1.81}3p^{3.71}3d^{0.01}4p^{0.01}$
N(I)	Au	1	-0.182	$6s^{0.91}5d^{9.66}6p^{0.59}7s^{0.01}6d^{0.01}$
	Au	2	0.199	$6s^{0.94}5d^{9.81}6p^{0.06}$
	P	3	0.059	$3s^{1.78}3p^{3.13}3d^{0.02}4p^{0.01}$
	P	4	0.107	$3s^{1.79}3p^{3.08}3d^{0.02}4p^{0.01}$
	P	5	-0.183	$3s^{1.85}3p^{3.32}3d^{0.01}4p^{0.01}$
C(II)	Au	1	-0.148	$6s^{0.93}5d^{9.64}6p^{0.56}$
	Au	2	0.384	$6s^{0.81}5d^{9.76}6p^{0.05}$
	P	3	0.260	$3s^{1.83}3p^{2.88}3d^{0.02}4p^{0.01}$
	P	4	0.208	$3s^{1.83}3p^{2.93}3d^{0.02}$
	P	5	0.296	$3s^{1.85}3p^{2.83}3d^{0.02}4p^{0.01}$

Table 3. **Topology analysis of the different valence states of Au_2P_3.** Electron Density ρ(r) [e·Å^{-3}], Electron Density Laplacian $\nabla^2\rho(r)$ [e·Å^{-5}], Eigenvalues of the Hessian Matrix (λ_1, λ_2 and λ_3), Lagrangian kinetic energy (G(r)) [Hartree·Å^{-3}], Potential energy density (ν(r)) [Hartree·Å^{-3}], Total Energy density (E(r)) [Hartree·Å^{-3}] and ellipticity ($\varepsilon = \lambda_1/\lambda_2-1$) at Bond Critical Points (BCPs).

Species	BCP	ρ(r)	$\nabla^2\rho$ (au)	λ_1	λ_2	λ_3	G(r)	ν(r)	E(r)	ε
A(I)	1-3	0.072	0.061	-0.058	-0.050	0.169	0.040	-0.064	-0.025	0.148
	1-4	0.072	0.061	-0.058	-0.050	0.169	0.040	-0.064	-0.025	0.148
	1-5	0.105	0.014	-0.096	-0.089	0.198	0.056	-0.108	-0.052	0.077
	2-5	0.086	0.005	-0.072	-0.070	0.148	0.041	-0.081	-0.040	0.024
	3-4	0.115	-0.103	-0.103	-0.098	0.098	0.038	-0.101	-0.063	0.053
N(I)	1-2	0.053	0.117	-0.036	-0.017	0.170	0.043	-0.056	-0.014	1.132
	1-3	0.080	0.055	-0.068	-0.055	0.179	0.044	-0.075	-0.031	0.219
	1-4	0.076	0.055	-0.064	-0.048	0.167	0.041	-0.069	-0.027	0.331
	1-5	0.099	-0.007	-0.086	-0.087	0.206	0.053	-0.098	-0.045	0.012
	2-5	0.090	-0.007	-0.079	-0.072	0.143	0.041	-0.083	-0.043	0.092
	3-4	0.144	-0.208	-0.132	-0.131	0.055	0.050	-0.152	-0.102	0.005
C(II)	1-3	0.072	0.049	-0.060	-0.049	0.158	0.037	-0.063	-0.025	0.209
	1-4	0.069	0.051	-0.056	-0.045	0.152	0.036	-0.059	-0.023	0.252
	1-5	0.108	0.060	-0.099	-0.095	0.254	0.066	-0.116	-0.050	0.040
	2-5	0.102	0.010	-0.094	-0.088	0.192	0.053	-0.103	-0.050	0.077
	3-4	0.119	-0.116	-0.109	-0.108	0.102	0.039	-0.106	-0.067	0.010

Figure Captions

Figure 1 The possible structural isomers, relative energies and molecular geometry symmetries of the low-lying isomers of $Au_2P_3^z$ (z = -1, 0, 1) at the PBE0/CRENBL level of theory. [a]

[a] *** labels indicate the isomers is chiral structure, respectively.**

Figure 2 The selected three isomers at different valence states (i.e., A(I), N(I), and C(II)) at the PBE0/CRENBL level of theory.

Figure 3 The frontier molecular orbitals of $Au_2P_3^z$ (z = -1, 0, 1).

Figure 4 Electron density deformation map of $Au_2P_3^z$ (z = -1, 0, +1). 4a and 4a' show the electron density deformation of $Au_2P_3^-$ (A(I)) corresponding to planes a and a' shown in the center of the figure. 4b and 4c show the electron density difference of Au_2P_3 (N(I)) and $Au_2P_3^+$ (C(II)). The solid and dashed lines represent the accumulated and depleted regions of electronic density, respectively.

Figure 5 The electron localization function (ELF) map of A(I), N(I), C(II). 5a and 5a' present the side (1-2-5 plane) and front (1-3-4 plane) of A(I), respectively. 5b and 5c show N(I) and C(II), respectively. The color range is (0, 1). The value equal to 0 corresponds to a delocalized system, whereas a value of 1 corresponds to a completely localized region. Core basins are located in nucleus and valence basins are characterized by their synaptic basins orders.

Figure 6 The ellipticity at the BCP of Au1-Au2 of the N(I).

Figure 7 The Reduced Density Gradient (RDG) analysis of the Au1-Au2 interaction.

Fig. 1

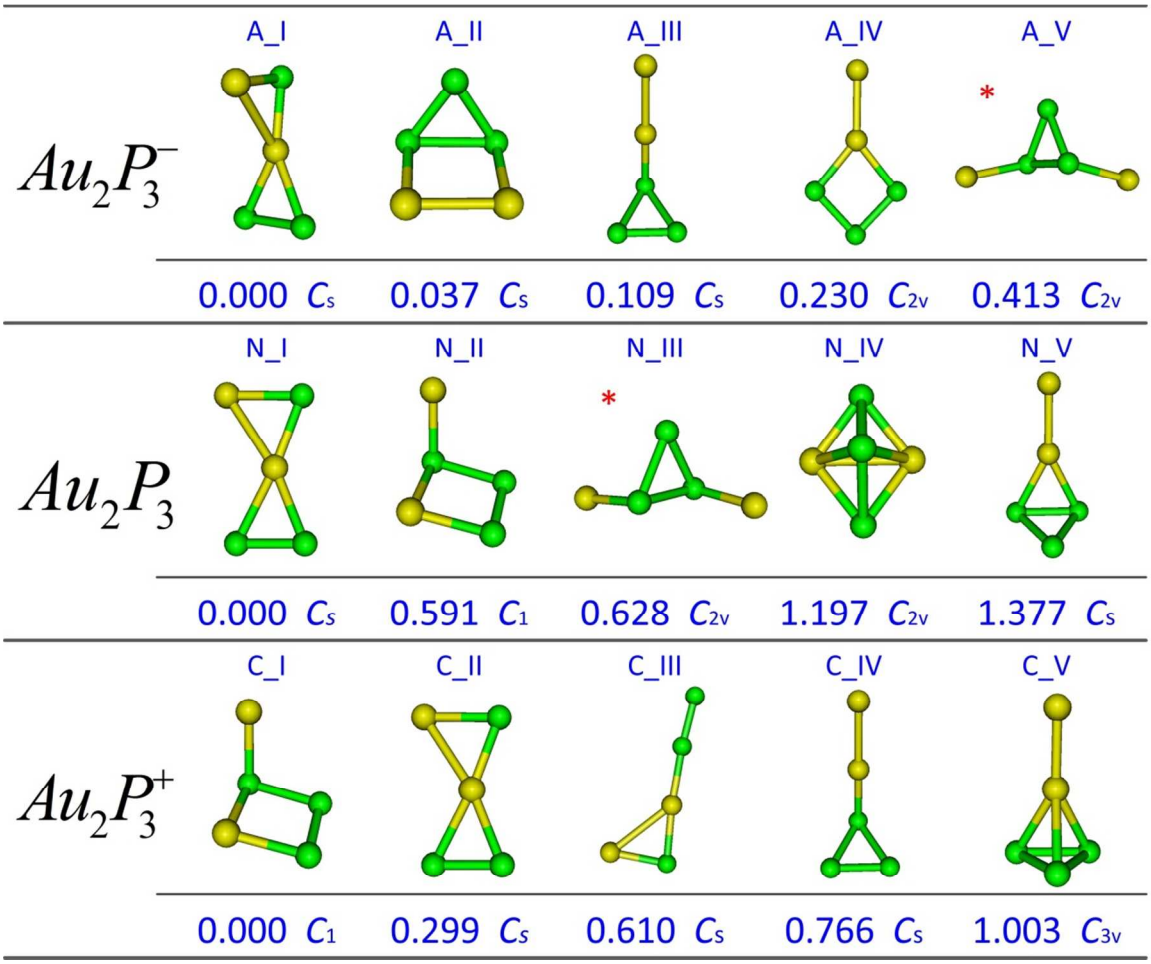

Fig. 2

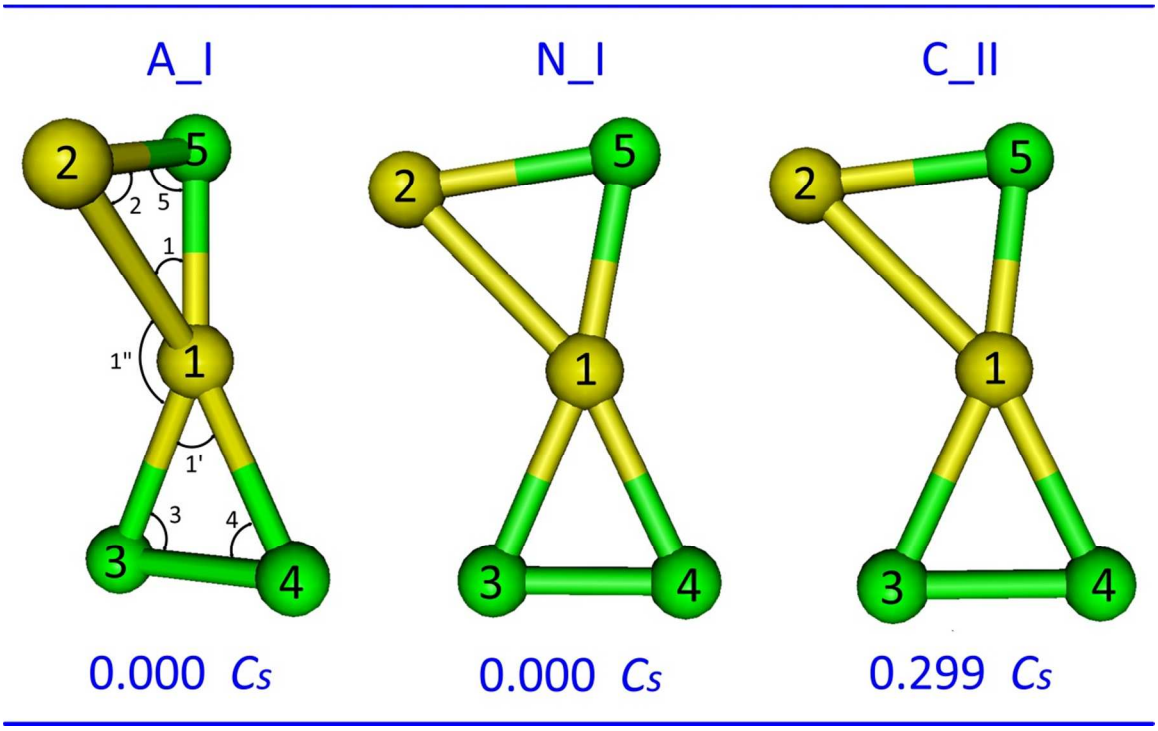

Fig. 3

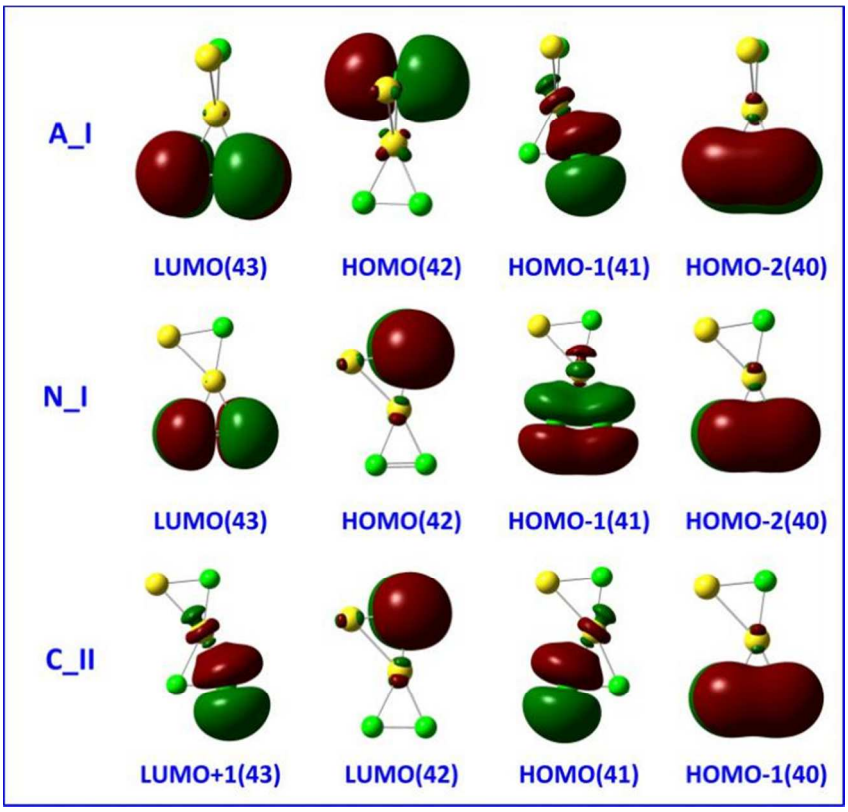

Fig. 4

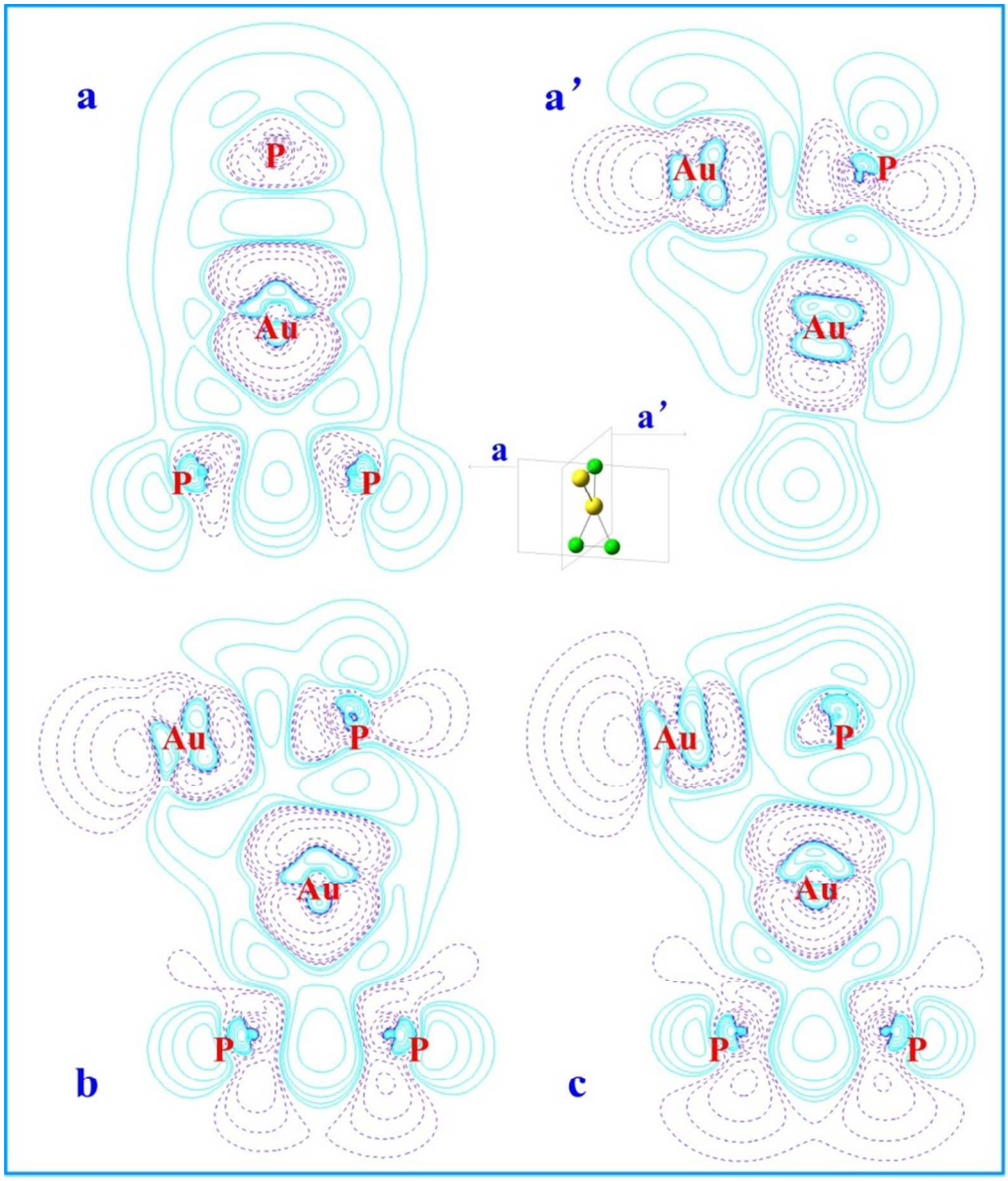

Fig. 5

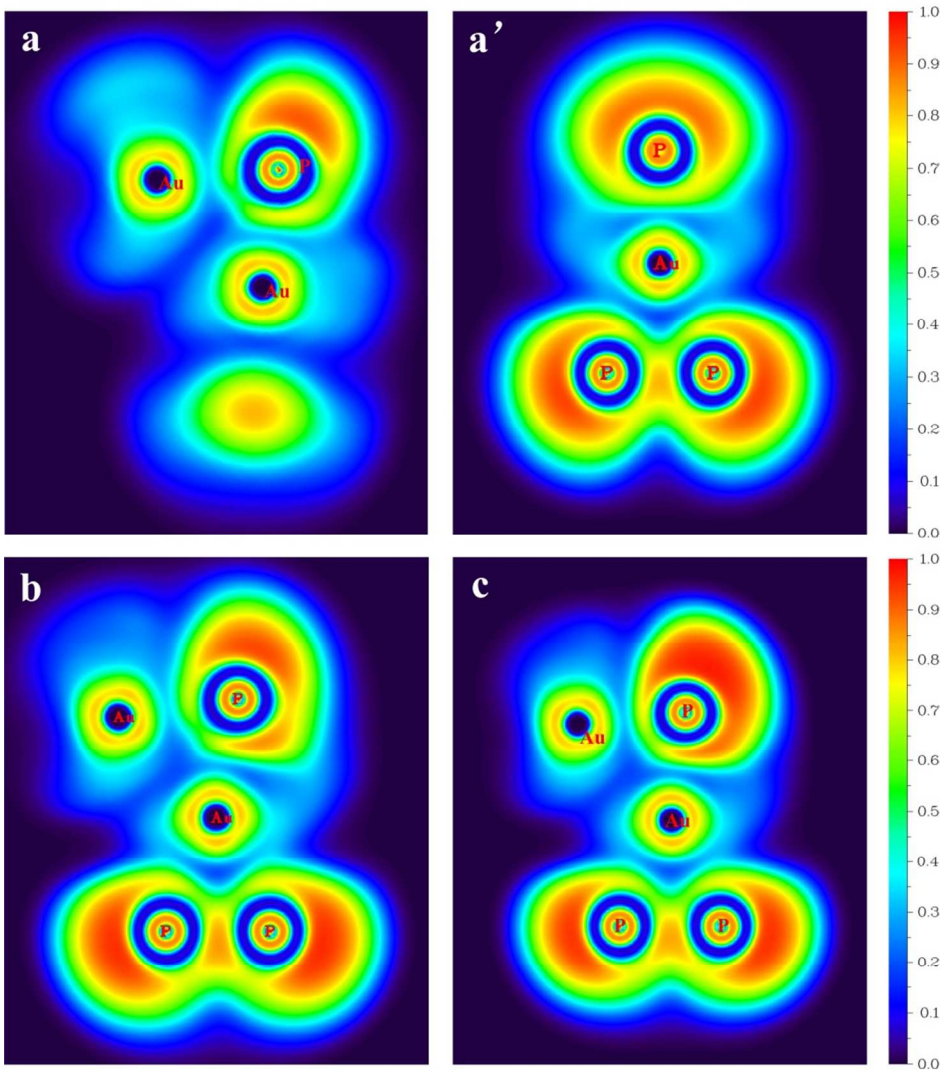

Fig. 6

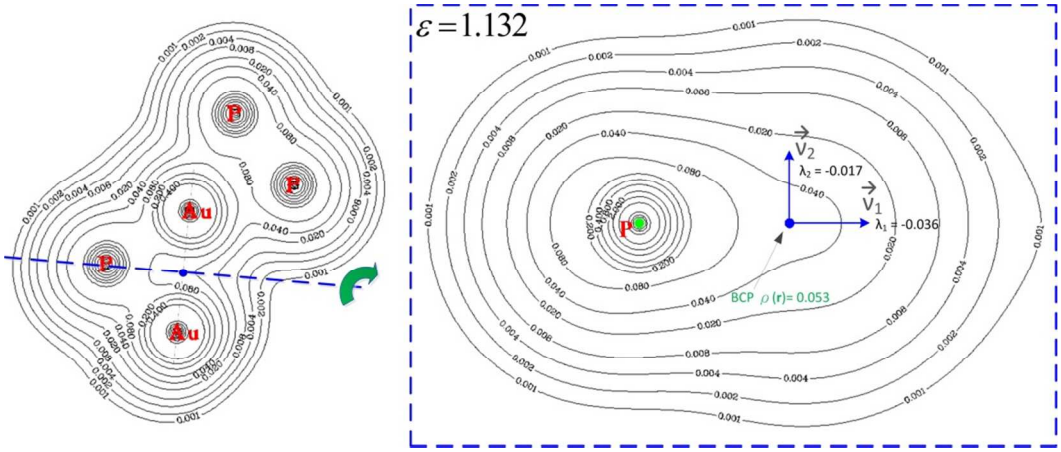

Fig. 7

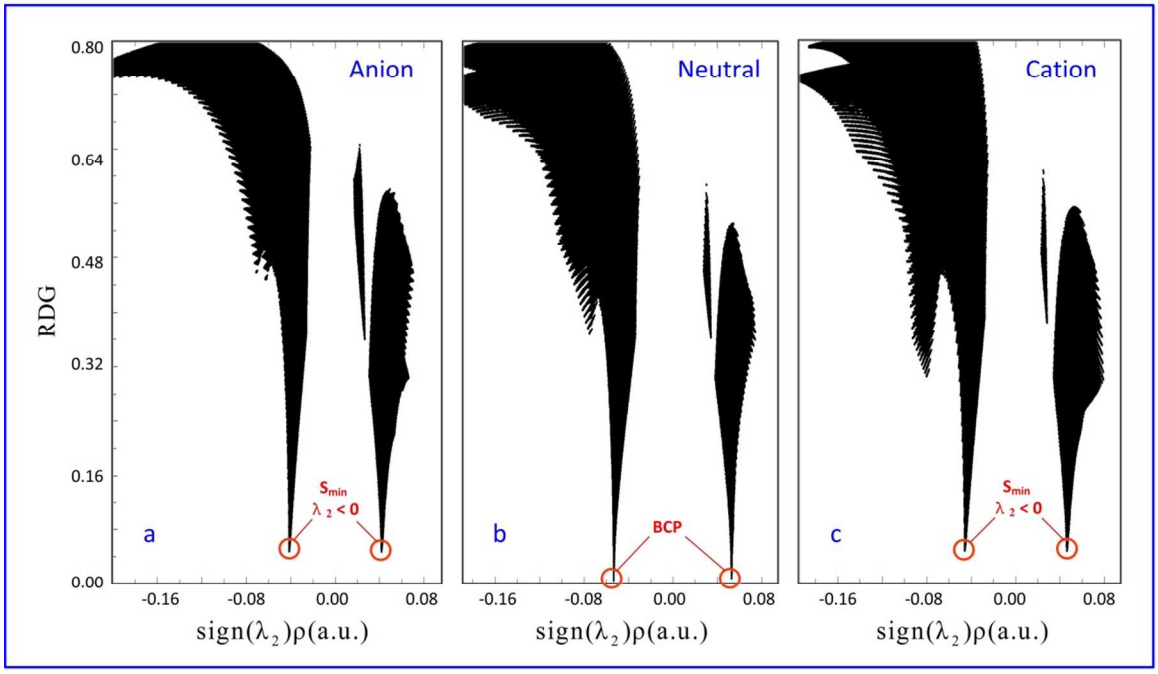

1. M. Sharon and G. Tamizhmani, J. Mater. Sci., 1986, 21, 2193-2201.
2. T. Trindade, P. O'Brien and N. L. Pickett, Chem. Mater., 2001, 13, 3843-3858.
3. S. T. Oyama, J. Catal., 2003, 216, 343-352.
4. H. Barz, H. Ku, G. Meisner, Z. Fisk and B. Matthias, Proc. Natl. Acad. Sci.USA, 1980, 77, 3132-3134.
5. M. V. Landau, M. Herskowitz, T. Hoffman, D. Fuks, E. Liverts, D. Vingurt and N. Froumin, Ind. Eng. Chem. Res., 2009, 48, 5239-5249.
6. S. L. Brock, S. C. Perera and K. L. Stamm, Chem. Eur. J., 2004, 10, 3364-3371.
7. S. T. Oyama, T. Gott, H. Zhao and Y. -K. Lee, Catal. Today, 2009, 143, 94-107.
8. A.-M. Alexander and J. S. Hargreaves, Chem. Soc. Rev., 2010, 39, 4388-4401.
9. Y. Kanda, C. Temma, K. Nakata, T. Kobayashi, M. Sugioka and Y. Uemichi, Appl. Catal. A, 2010, 386, 171-178.
10. S. Pyshkin, J. Ballato, M. Bass and G. Turri, J. Electron. Mater., 2009, 38, 640-646.
11. J. Cabana, L. Monconduit, D. Larcher and M. R. Palacin, Adv. Mater., 2010, 22, E170-E192.
12. M. G. Kim and J. Cho, Adv. Funct. Mater., 2009, 19, 1497-1514.
13. I. Shein, N. Medvedeva and A. Ivanovskii, Physica B, 2006, 371, 126-132.
14. P. Pyykko, Chem. Soc. Rev., 2008, 37, 1967-1997.
15. P. Pyykko, Inorg. Chim. Acta, 2005, 358, 4113-4130.
16. P. Pyykko, Angew. Chem. Int. Edit., 2004, 43, 4412-4456.
17. A. Allred, J. Inorg. Nucl. Chem., 1961, 17, 215-221.
18. E. J. Fernandez, A. Laguna and M. E. Olmos, J. Chil. Chem. Soc., 2007, 52, 1200-1205.
19. A. I. Kozlov, A. P. Kozlova, H. C. Liu and Y. Iwasawa, Appl. Catal. A, 1999, 182, 9-28.
20. W. Jeitschko and M. H. Moller, Acta Crystallogr., Sect. B, 1979, 35, 573-579.
21. M. Eschen and W. Jeitschko, J. Solid State Chem., 2002, 165, 238-246.
22. V. G. Weizer and N. S. Fatemi, J. Appl. Phys., 1991, 69, 8253-8260.
23. A. E. Henkes, Y. Vasquez and R. E. Schaak, J. Am. Chem. Soc., 2007, 129, 1896-+.
24. Z. Y. Liu, R. B. Huang and L. S. Zheng, Chem. J. Chinese U., 1997, 18, 293-296.
25. N. R. Panyala, E. M. Pena-Mendez and J. Havel, Rapid Commun. Mass Spectrom., 2012, 26, 1100-1108.
26. S. Carenco, I. Florea, O. Ersen, C. Boissiere, N. Mezailles and C. Sanchez, New J. Chem., 2013, 37, 1231-1237.
27. X.-D. Wen, T. J. Cahill and R. Hoffmann, J. Am. Chem. Soc., 2009, 131, 2199-2207.
28. Y. Li, Y. P. Cao, Y. F. Li, S. P. Shi and X. Y. Kuang, Eur. Phys. J. D, 2012, 66.
29. G. F. Zhao, Y. L. Wang, J. M. Sun and Y. X. Wang, Acta Phy-Chim Sin., 2012, 28, 1355-1360.
30. M. Zhang, S. Chen, Q. M. Deng, L. M. He, L. N. Zhao and Y. H. Luo, Eur. Phys. J. D, 2010, 58, 117-123.
31. C. Majumder, A. K. Kandalam and P. Jena, Phys. Rev. B, 2006, 74.
32. K. M. Xu, T. Huang, H. Wen, Y. R. Liu, Y. B. Gai, W. J. Zhang and W. Huang, RSC Adv., 2013, 3, 24492-24502.
33. K. M. Xu, T. Huang, Y. R. Liu, S. Jiang, Y. Zhang, Y. Z. Lv, Y. B. Gai and W. Huang, J. Phys. Chem. A, 2014, [revised]
34. O. Olofsson, Acta Chem. Scand., 1970, 24, 723.
35. H. Okamoto and T. Massalski, J. Phase Equilib., 1984, 5, 490-491.
36. M. Eschen, J. Wallinda and W. Jeitschko, Z. Anorg. Allg. Chem., 2002, 628, 2764-2771.
37. M. Eschen, G. Kotzyba, B. Kunnen and W. Jeitschko, Z. Anorg. Allg. Chem., 2001, 627, 1699-1708.
38. S. Carenco, D. Portehault, C. Boissiere, N. Mezailles and C. Sanchez, Chem. Rev., 2013, 113, 7981-8065.
39. H. Haraldsen and W. Biltz, Z. Elektrochem., 1931, 37, 504-506.
40. S. H. Yoo and X. C. Zeng, Angew. Chem. Int. Edit., 2005, 44.
41. D. J. Wales and J. P. K. Doye, J. Phys. Chem. A, 1997, 101.

42. W. Huang, R. Pal, L. M. Wang, X. C. Zeng and L. S. Wang, J. Chem. Phys., 2010, 132, 054305.
43. S. Yoo and X. C. Zeng, J. Chem. Phys., 2003, 119.
44. Y. R. Liu, H. Wen, T. Huang, X. X. Lin, Y. B. Gai, C. J. Hu, W. J. Zhang and W. Huang, J. Phys. Chem. A, 2014, 118, 508-516.
45. J. P. Perdew, K. Burke and M. Ernzerhof, Phys. Rev. Lett., 1996, 77, 3865-3868.
46. B. Delley, J. Chem. Phys., 1990, 92, 508-517.
47. H. Wen, Y. R. Liu, K. M. Xu, T. Huang, C. J. Hu, W. J. Zhang and W. Huang, RSC Adv., 2014, 4, 15066-15076.
48. L. L. Yan, Y. R. Liu, T. Huang, S. Jiang, H. Wen, Y. B. Gai, W. J. Zhang and W. Huang, J. Chem. Phys., 2013, 139, 244312.
49. H. Wen, Y. R. Liu, T. Huang, K. M. Xu, W. J. Zhang, W. Huang and L. S. Wang, J. Chem. Phys., 2013, 138, 174303.
50. W. Huang, H. J. Zhai and L. S. Wang, J. Am. Chem. Soc., 2010, 132, 4344-4351.
51. W. Huang and L. S. Wang, Phys. Chem. Chem. Phys., 2009, 11, 2663-2667.
52. W. Huang, S. Bulusu, R. Pal, X. C. Zeng and L. S. Wang, ACS Nano, 2009, 3, 1225-1230.
53. W. Huang, S. Bulusu, R. Pal, X. C. Zeng and L. S. Wang, J. Chem. Phys., 2009, 131.
54. C. Adamo and V. Barone, J. Chem. Phys., 1999, 110, 6158.
55. R. A. Kendall, E. Apra, D. E. Bernholdt, E. J. Bylaska, M. Dupuis, G. I. Fann, R. J. Harrison, J. L. Ju, J. A. Nichols, J. Nieplocha, T. P. Straatsma, T. L. Windus and A. T. Wong, Comput. Phys. Commun., 2000, 128, 260-283.
56. E. J. Bylaska, W. A. de Jong, N. Govind, K. Kowalski, T. P. Straatsma, M. Valiev, D. Wang, E. Apra, T. L. Windus, J. Hammond, P. Nichols, S. Hirata, M. T. Hackler, Y. Zhao, P.-D. Fan, R. J. Harrison, M. Dupuis, D. M. A. Smith, J. Nieplocha, V. Tipparaju, M. Krishnan, Q. Wu, T. Van Voorhis, A. A. Auer, M. Nooijen, E. Brown, G. Cisneros, G. I. Fann, H. Fruchtl, J. Garza, K. Hirao, R. Kendall, J. A. Nichols, K. Tsemekhman, K. Wolinski, J. Anchell, D. Bernholdt, P. Borowski, T. Clark, D. Clerc, H. Dachsel, M. Deegan, K. Dyall, D. Elwood, E. Glendening, M. Gutowski, A. Hess, J. Jaffe, B. Johnson, J. Ju, R. Kobayashi, R. Kutteh, Z. Lin, R. Littlefield, X. Long, B. Meng, T. Nakajima, S. Niu, L. Pollack, M. Ros-ing, G. Sandrone, M. Stave, H. Taylor, G. Thomas, J. van Lenthe, A. Wong, and Z. Zhang,NWChem, A Computational Chemistry Package for Parallel Computers, Version 5.1 (Pacific Northwest National Laboratory, Richland, 2009).
57. A. E. Reed, R. B. Weinstock and F. Weinhold, J. Chem. Phys., 1985, 83, 735-746.
58. M. J. Frisch, G. W. Trucks, H. B. Schlegel, G. E. Scuseria, M. A. Robb, J. R. Cheeseman, G. Scalmani, V. Barone, B. Mennucci, G. A. Petersson, H. Nakatsuji, M. Caricato, X. Li, H. P. Hratchian, A. F. Izmaylov, J. Bloino, G. Zheng, J. L. Sonnenberg, M. Hada, M. Ehara, K. Toyota, R. Fukuda, J. Hasegawa, M. Ishida, T. Nakajima, Y. Honda, O. Kitao, H. Nakai, T. Vreven, J. A. Montgomery Jr., J. E. Peralta, F. Ogliaro, M. J. Bearpark, J. Heyd, E. N. Brothers, K. N. Kudin, V. N. Staroverov, R. Kobayashi, J. Normand, K. Raghavachari, A. P. Rendell, J. C. Burant, S. S. Iyengar, J. Tomasi, M. Cossi, N. Rega, N. J. Millam, M. Klene, J. E. Knox, J. B. Cross, V. Bakken, C. Adamo, J. Jaramillo, R. Gomperts, R. E. Stratmann, O. Yazyev, A. J. Austin, R. Cammi, C. Pomelli, J. W. Ochterski, R. L. Martin, K. Morokuma, V. G. Zakrzewski, G. A. Voth, P. Salvador, J. J. Dannenberg, S. Dapprich, A. D. Daniels, Ö. Farkas, J. B. Foresman, J. V. Ortiz, J. Cioslowski and D. J. Fox, Gaussian 09, (2009) Gaussian, Inc., Wallingford, CT, USA.
59. B. Silvi and A. Savin, Nature, 1994, 371, 683-686.
60. A. D. Becke and K. E. Edgecombe, J. Chem. Phys., 1990, 92, 5397-5403.
61. E. R. Johnson, S. Keinan, P. Mori-Sanchez, J. Contreras-Garcia, A. J. Cohen and W. T. Yang, J. Am. Chem. Soc., 2010, 132, 6498-6506.
62. J. S. Binkley and J. A. Pople, Inter. J. Quant. Chem., 1975, 9, 229-236.
63. T. Lu and F. Chen, J. Comput. Chem., 2012, 33, 580-592.

64. F. Furche, R. Ahlrichs, P. Weis, C. Jacob, S. Gilb, T. Bierweiler and M. M. Kappes, J. Chem. Phys., 2002, 117, 6982-6990.
65. D. R. Lide (ed.): *CRC handbook of chemistry and physics, CD-ROM Version 2005*: CRC Press, Boca Raton, 2005.
66. A. Becke, C. F. Matta and R. J. Boyd, The quantum theory of atoms in molecules: from solid state to DNA and drug design, John Wiley & Sons, 2007.
67. R. F. Bader, Atoms in molecules, Wiley Online Library, 1990.
68. W. Nakanishi, S. Hayashi and K. Narahara, J. Phys. Chem. A, 2008, 112, 13593-13599.